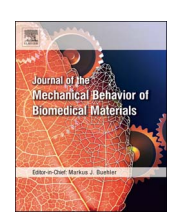
FISEVIER

Contents lists available at ScienceDirect

# Journal of the Mechanical Behavior of Biomedical Materials

journal homepage: www.elsevier.com/locate/jmbbm



# Atomic force microscopy study revealed velocity-dependence and nonlinearity of nanoscale poroelasticity of eukaryotic cells



Keyvan Mollaeian, Yi Liu, Siyu Bi, Juan Ren\*

Department of Mechanical Engineering, Iowa State University, Ames, IA 50011, USA

#### ARTICLE INFO

Keywords: Cell rheology Poroelasticity AFM Velocity-dependency Nonlinearity

### ABSTRACT

Intracellular network deformation of the cell plays an important role in cellular shape formation. Recent studies suggest that cell reshaping and deformation due to external forces involve cellular volume, pore size, elasticity, and intracellular filaments polymerization degree change. This cell behavior can be described by poroelastic models due to the porous structure of the cytoplasm. In this study, the nanoscale poroelasticity of human mammary basal/claudin low carcinoma cell (MDA-MB-231) was investigated using indentation-based atomic force microscopy. The effects of cell deformation (i.e., indentation) velocity and depth on the poroelasticity of MDA-MB-231 cells were studied. Specifically, the cell poroelastic behavior (i.e., the diffusion coefficient) was quantified at different indenting velocities (0.2, 2, 10, 20, 100, 200 µm/s) and indentation depths (635, 965, and 1313 nm) by fitting the force-relaxation curves using a poroelastic model. Cell treated with cytoskeleton inhibitors (latrunculin B, blebbistatin, and nocodazole) were measured to investigate the effect of the cytoskeletal components on the cell poroelasticity. It was found that in general the MDA-MB-231 cells behaved less poroelastic (i.e., with lower diffusion coefficient) at higher indenting velocities due to the local stiffening up and dramatic pore size reduction caused by faster force load, and the cytoplasm is nonlinear in terms of poroelasticity. The poroelastic relaxation was more pronounced when the local cytoplasm porous structure was stretched by higher indentation. Furthermore, inhibition of cytoskeletal components resulted in pronounced poroelastic relaxation when compared with the control, and affected the nonlinearity of cell poroelasticity at different depth range inside of the cell. The comparison between the diffusion coefficient variation and the Young's modulus change under each indentation/treatment condition suggested that the cytoplasm porous geometry is more dominant than the cell Young's modulus in terms of affecting cell poroelasticity.

#### 1. Introduction

Nowadays, attention toward cell rheology is growing due to the sensitivity of cell shape and deformation to external and internal biomechanical stimulation. For example, internal induced-forces due to biochemical interaction, intracellular organelle transport (Niclas et al., 1996), transcriptional change of genes (Coller et al., 2000), and signaling pathways (Elledge, 1996) proceed to elongation of the cells and cell cycling. Mutation of the genes, adapted pathways, and chemical interactions in different cell lines such as cancerous cells lead to significant cell rheological behavior change (Moeendarbary and Harris, 2014; Maloney et al., 2010; Sun et al., 2012; Brandao et al., 2003). Moreover, integrin-mediated focal adhesion (Balaban et al., 2001; Plotnikov et al., 2012), ion channels (Hayakawa et al., 2008), and cytoskeleton of the cell (Mitrossilis et al., 2009; Colombelli et al., 2009; Hayakawa et al., 2011) are responsive to extracellular forces applied on the cell. As cytoplasm forms the largest part of a cell by volume, its

biomechanical property plays a key role in cell rheology by dictating the cell deformation magnitude and cell shape change rate. Therefore, investigating the biomechanical behavior of the cytoplasm is crucial in achieving in-depth understanding of cell rheology. Furthermore, as it is widely found that living cells probe, react, and adapt to external mechanical stimulation (Moeendarbary et al., 2013; Schillers et al., 2010), studying the mechanical properties of cytoplasm also promotes the modeling and quantification of the transduction of external mechanical stimulation into intracellular mechanical changes (Zhu et al., 2016; Charras et al., 2005, 2009).

Classical mechanical models have been implemented to biomechanics investigation of cell cytoplasm. The cortical shellliquid core models (e.g., the Newtonian liquid drop model (Tran-Son-Tay et al., 1991; Yeung and Evans, 1989), the compound Newtonian liquid drop model (Dong et al., 1990; Hochmuth et al., 1993), the shear thinning liquid drop model (Drury and Dembo, 1999, 2001), and the Maxwell liquid drop model (Sung and Schmid-Schb, 1988)) were developed to

E-mail address: juanren@iastate.edu (J. Ren).

<sup>\*</sup> Corresponding author.

describe the rheology of cytoplasm in micropipette aspiration by assuming the homogeneity of the cell layer structure (Lim et al., 2006; Evans and Kukan, 1984; Yeung and Evans, 1989). To study the mechanics of cytoskeleton, solid models, such as the Hertzian model and the Sneddon model can be used to describe the contact mechanics between an elastic indenter and living cells by assuming the latter as an elastic isotropic body, and the contact is purely repulsive (Liu, 2006; Butt et al., 2005; Ghaednia et al., 2015a, 2016; Jackson et al., 2015). Due to the existence of attractive forces (e.g, van der Waals forces) when the indenters are brought into close proximity with the cells, the Johnson-Kendall-Roberts (JKR) (Chu et al., 2005) and the Deriaguin-Muller-Toporov (DMT) (Gao and Yao, 2004) models were then used to incorporate the effect of adhesion in Hertzian contact by taking the thermodynamic work of adhesion into account (Johnson et al., 1971; Derjaguin et al., 1975; Wu, 1982). The power-law structural damping model (Hildebrandt, 1969; Fredberg and Stamenovic, 1989; Maksym et al., 2000; Fabry et al., 2001; Kardel et al., 2017; Ghaednia et al., 2015b) was used for studying the viscoelasticity and the dynamic behavior of adherent cells (Ren et al., 2013). However, these models are not adequate enough to describe the biomechanical behavior of both the liquid flow (e.g., the cytosol) and the viscoelastic network (e.g., the cytoskeleton) —the biphasic nature of the cytoplasm. Therefore, a poroelastic model was implemented to study the biomechanics of cytoplasm, in which the cytoplasm was considered as a biphasic material consisting of a porous elastic solid meshwork (cytoskeleton, organelles, macromolecules) bathed in an interstitial fluid (cytosol) (Oster, 1989; Gu et al., 1997; Bachrach et al., 1995; Guilak and Mow, 2000; Moeendarbary et al., 2013). In the poroelastic model, the response of cells to external force load depends only on the poroelastic diffusion coefficient, D, which is determined by E the elastic modulus,  $\xi$  the pore size of the cytoskeleton meshwork, and  $\mu$  the viscosity of the cytosol (Moeendarbary et al., 2013; Charras et al., 2009, 2008). According to the coarse graining of the physical parameters in the poroelastic model, cellular rheology results from the effects of the interstitial fluid (Keren et al., 2009), the related cell volume changes (Moeendarbary et al., 2013; CHENG), macromolecular crowding and the cytoskeletal network (Moeendarbary et al., 2013; Schillers et al., 2010), this is consistent with the observed rheological properties of the cell that the internal cell pressure equilibrates by redistribution of intracellular fluids in response to localized deformation (Charras et al., 2005, 2009; Keren et al., 2009; Rosenbluth et al., 2008; Zicha et al., 2003).

Poroelasticity studies of eukaryotic cells have been performed on atomic force microscopy (AFM) because of AFM's unique capability of applying force stimuli and then, measuring the sample response at specific locations in a physiologically friendly environment with piconewton force and nanometer spatial resolutions (Giridharagopal et al., 2012; Yan et al., 2017; Efremov et al., 2017). Weafer et al. (2015) investigated the force generation of the cells under an applied constant cyclic loading and unloading nominal strain rate at a frequency of 1 Hz, and it was found that the compression force was recovered and reached equilibrium at end of last cycle. Weafer et al. (2015). Hu et al. (2010) reported that interaction force between the AFM tip and the hydrogels was decreased during relaxation of the tip on the sample which led to deformation of the hydrogels (Hu et al., 2010). Tavakoli Nia et al. (2011) noted the poroelastic behavior of cartilage during relaxation experiment using AFM (Nia et al., 2011). It has been noted that the mechanical response of fluid-filled materials, like cells, depends on the time and length scales of the measurements and the mechanical deformation of the materials changes during the entire experimental time span (Kalcioglu et al., 2012). Moeendarbary et al. (2013) investigated the poroelastic behavior of the cell using micro bead when the approach velocity was 10 μm/s, and it was found that the components of the cells including actin, microtubules, myosin, and intermediate filaments affect the diffusion coefficient of the cell (Moeendarbary et al., 2013). However, since the cytoplasm of a living cell is highly heterogeneous and consists of a multi-layer structured viscoelastic cytoskeleton (i.e.,

velocity dependent), the cytoplasm poroelasticity quantified in previous work was limited to the specific measurement specifications and physical conditions (e.g., indenter size, approach velocity, and indentation depth). Particularly, due to the biphasic nature of living cells, the cell deformation rate (i.e., the AFM probe approach velocity) affects the measured cell stiffness significantly (Moeendarbary et al., 2013; CHENG), and the deformation/indentation depth range determined the layers of the cells triggered and measured during the mechanical quantification (Kasas et al., 2005; Fuhrmann et al., 2011). Thus, to achieve in-depth understanding of the cell rheological behavior, study the poroelastic behavior of cytoplasm under different external excitation conditions is necessary.

In this study, we investigated the contribution of external force conditions to cellular rheology of human mammary basal/claudin low carcinoma cell at nanometer scale using AFM. Specifically, the cells were probed under forces with different approach velocities and magnitudes, and the poroelasticity diffusion coefficient was then quantified for each condition by fitting the force-relaxation curve using an empirical poroelastic model. Furthermore, to study the effect of internal cell structural property on determining the cell rheology and the nonlinearity of cell poroelasticity, we examined the importance of cytoskeleton in affecting cell poroelasticity.

#### 2. Materials and methods

#### 2.1. Chemicals

The human mammary basel/claudin low carcinoma cell line (MDA-MB-231) and Leibovitz's L-15 Medium (L-15) were purchased from American Type Culture Collection (ATCC, Rockville, MD, USA). Dubecco's Modified Eagles Medium (DMEM) and Dimethyl sulfoxide (DMSO) were purchased from Sigma Aldrich (St. Louis, MO, USA). Fetal bovine serum and penicillin-streptomycin were obtained from Gibco (Grand Island, New York, USA). Latrunculin B and blebbistatin were purchased from Millipore sigma (Billerica, Massachusetts, USA). Nocodazole was purchased from Acros organics (New Jersey, USA).

# 2.2. Cell culture and treatment

MDA-MB-231 cells were cultured in the following cell growth medium: DMEM containing 10% fetal bovine serum (FBS) and 1% penicillin-steptomycin (pen-strep). The cells were subcultured at a density of  $2.0 \times 10^4$  cells/ml on 35 mm cell culture dishes (Falcon, Durham, NC, USA) and maintained at 37  $^\circ$  C in 5% CO $_2$  incubator 24 h prior to the AFM measurement. For the AFM poroelasticity measurements, the existing medium in the dishes was replaced by L-15 with the same concentration of FBS and pen-strep to remove dead and loosely attached cells, and to maintain the health of the cells during the experiment.

# 2.3. Cytoskeleton treatments

To investigate the contribution of cytoskeleton components on cell poroelasticity, the cells were treated with latrunculin B (750 nM to depolymerize F-actin), nocodazole (5  $\mu$  M to depolymerize microtubules), and blebbistatin (100  $\mu$ M to inhibit myosin II ATPase) separately in the aforementioned cell growth medium and incubated 30 min prior to the AFM measurements (Moeendarbary et al., 2013). Then, the cell growth medium was replaced by L-15 with 10% FBS, 1% pen-strep, and the same drug concentration such that the drug effect was present during all measurements. Stock solutions were made by dissolving each drug in DMSO. Then, the aforementioned stock concentrations were prepared by adding the medium dropwise into the solution (Mikulich et al., 2012). The DMSO concentration during the treatments and AFM measurement was 0.05%. To study the effects of the treatments on cell poroelasticity, the untreated cells were exposed to the same DMSO concentration, and used as control.

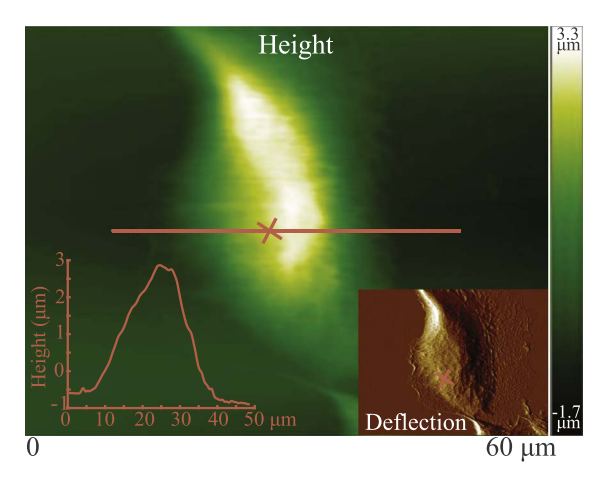


Fig. 2. AFM topography image of a MDA-MB-231 cell, where the red cross denotes the poroelasticity measurement.

### 2.4. Atomic Force Microscopy (AFM) measurement

AFM measurement was performed at room temperature in aforementioned medium on a Bruker BioScope Resolve AFM system (Santa Barbara, CA, USA), which was integrated with an inverted optical microscope (Olympus, IX73, Japan). MLCT-BIO-DC-C (Bruker, Camarillo, CA) probe was used to measure the cells, and the spring constant of 0.03 N/m was acquired using thermal tune approach (Hutter and Bechhoefer, 1993). During the experiment, the AFM probe (guided by

the optical microscope camera) was in contact with the cells at locations away from the top of the cells to avoid the nucleus effect. As an example, the AFM topography image of one cell measured during the experiment is shown in Fig. 2, where the measurement location on the cell and the cross-section are also shown. All of the AFM drive voltage and sensor data were acquired using an NI PCIe-6353 DAQ board (National Instrument, Austin, TX, USA) with Matlab Simulink Desktop Real-Time system (Mathworks, MA, USA).

As the cell poroelasticity is caused by intracellular fluid redistribution to equilibrate the intracellular pressure, to experimentally quantify the cell poroelastic behavior, the local cell internal pressure needs to be suddenly disturbed to trigger the intracellular fluid redistribution. Therefore, rapid AFM indentation was chosen in this study to disturb the cells, and the effects of both the loading speed and amplitude were studied. To investigate the effect of indenting speed (i.e., AFM probe approaching velocity) on poroelasticity of MDA-MB-231 cells, the AFM probe was brought into contact with the cells at six different speeds  $(0.2, 2.0, 10.0, 20.0, 100.0, and 200.0 \mu m/s)$  until reaching a target indentation of 960 nm (as illustrated in Fig. 3 (I-II)), and then the AFM z-piezo displacement was maintained constant at the corresponding value for 1 s to acquire the force relaxation data (Fig. 3 (II-III)). To investigate the effect of indentation depth on the poroelastic behavior of MDA-MB-231 cell, the approaching speed of the probe was kept at  $10 \mu m/s$  until the desired indentations were reached (635, 965, and 1313 nm). A proportional-integral (PI) feedback control loop was implemented to control the AFM piezo displacement. For each desired indenting velocity and indentation depth, the force measurement was performed on at least six different cells using the same AFM probe.

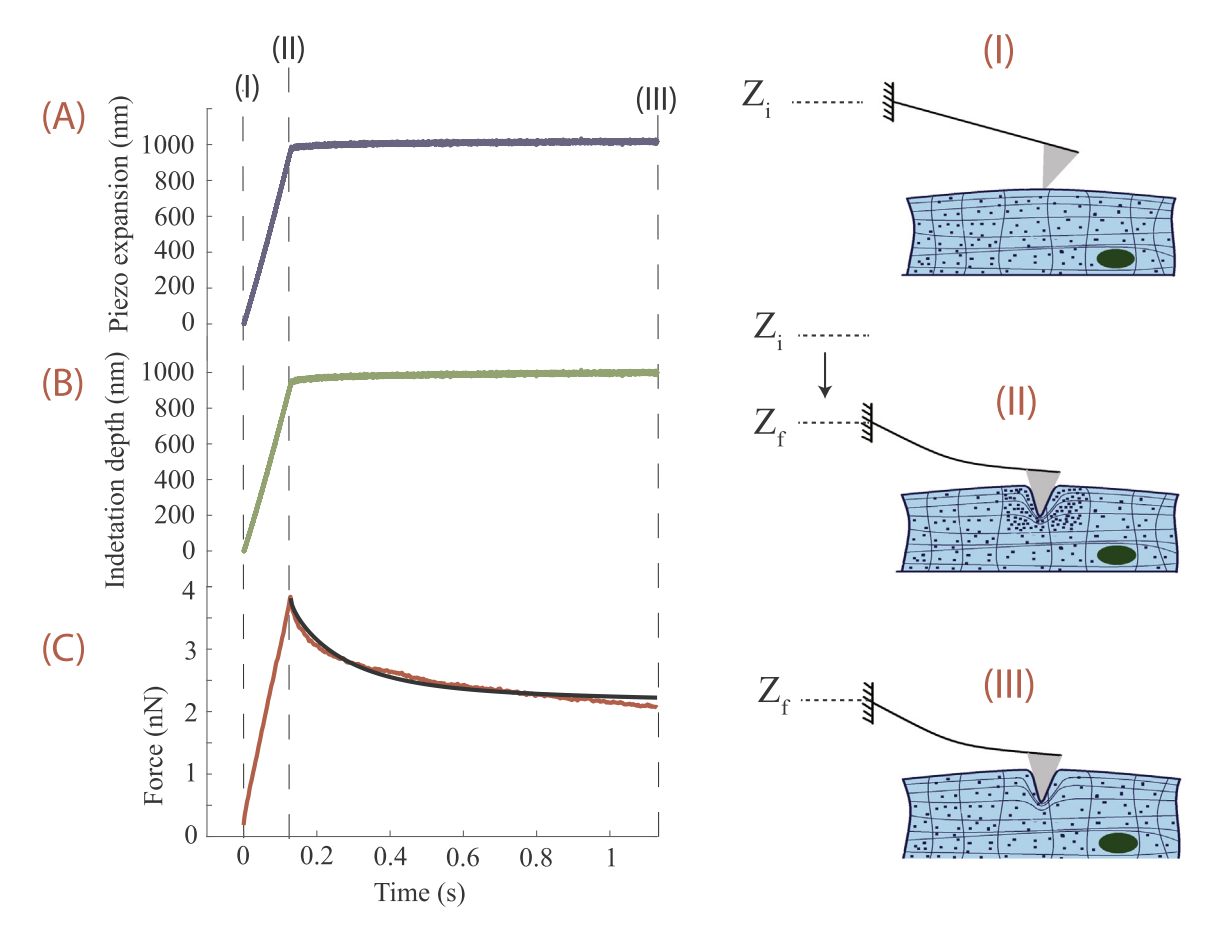


Fig. 3. (A, B, C) The AFM piezo displacement, the indentation depth, and the probe-sample interaction force during the poroelasticity measurement: I) At the beginning of the measurement the AFM tip was in contact with the surface of the cell with zero velocity. II) Indenting: the AFM probe indented the cell at a constant velocity until the desired indentation was reached. Multiple layers and the intracellular fluid of the cell were compressed during this loading process. III) Relaxation: the AFM probe rested on the cell, and the intracellular fluid redistributed to equilibrate the cell internal pressure, while the AFM z-piezo displacement was maintained at a constant since the end of the indenting process. The force-relaxation curve (the black solid curve in (C)) was then fitted using the poroelastic model.

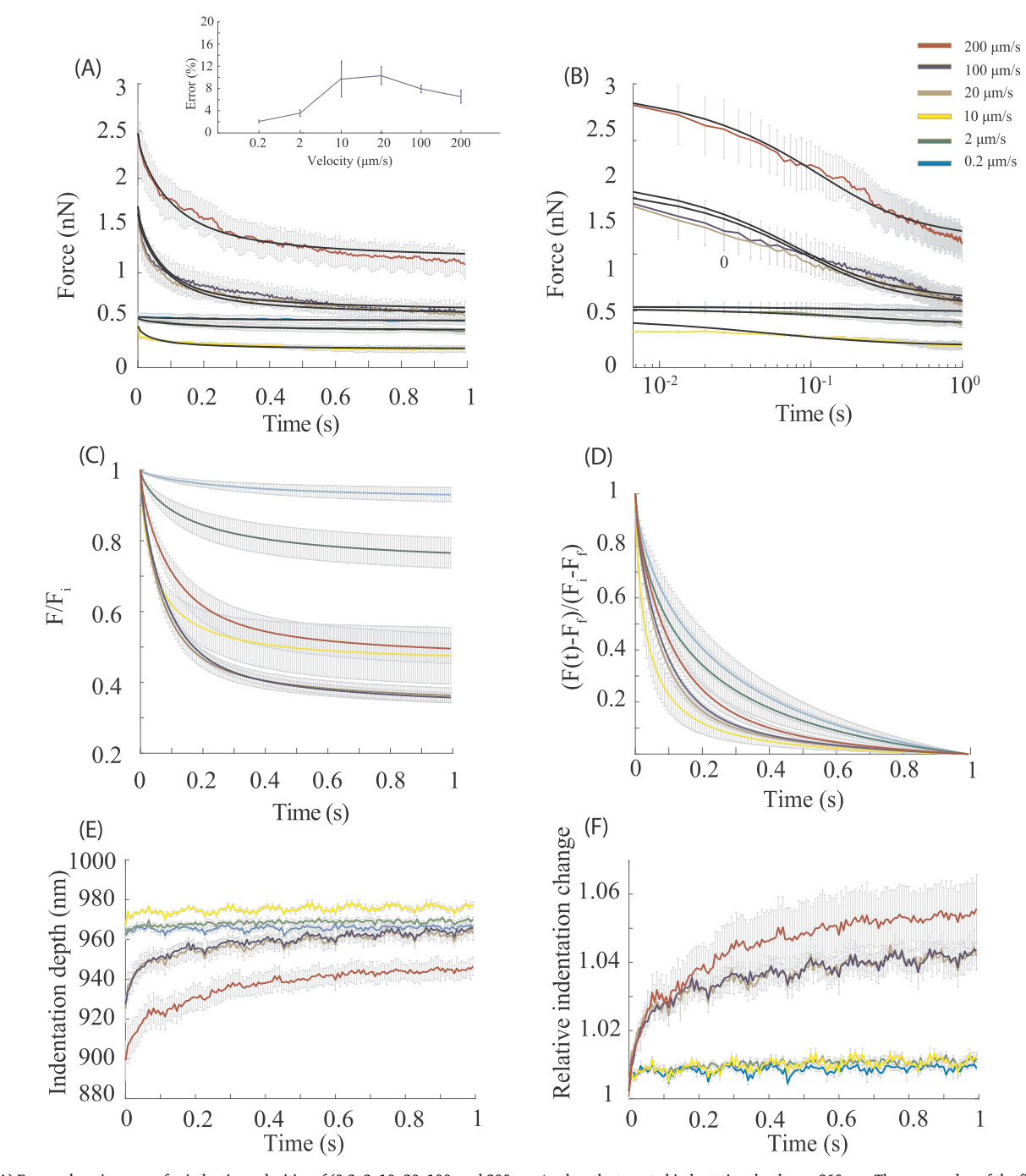


Fig. 4. (A) Force-relaxation curve for indenting velocities of (0.2, 2, 10, 20, 100, and 200  $\mu$ m/s when the targeted indentation depth was 960 nm. The mean value of the fitted curves for each velocity was shown as solid lines. The error bars denote the raw force data for each indenting velocity. (B) Log-Log plots of (A). (C) Relative force reduction during the relaxation process of the poroelastic fitted results in (A). (D) Normalized force reduction curve for different indenting velocities when the indentation depth was 960 nm. At the same time instant, lower normalized value denotes faster poroelastic relaxation. (E) Indentation change during the relaxation process: the indentation depth gradually increased when the probe was resting on the cell following the rapid indenting process. (F) Relative indentation change  $\delta/\bar{\delta}$  during the relaxation process.

## 2.5. Nanomechanical quantification of MDA-MB-231 cell

Indentation depth was calculated by subtracting the cantilever deflection, d(t), from the displacement of the AFM z-piezo displacement (Ren et al., 2015), z(t) i.e.,

$$\delta(t) = z(t) - d(t). \tag{1}$$

Since the AFM probe used had a conical shape, the Young's Modulus of MDA-MB-231 cells was quantified using the Sneddon model (Sneddon, 1965), i.e.,

$$F(t) = \frac{2}{\pi} \tan(\alpha) \frac{E}{1 - \nu^2} \delta^2(t). \tag{2}$$

where  $\alpha$  and  $\nu$  are the tip opening angle and the Poisson ratio of the cell, respectively. Additionally, the Poisson's ratio  $\nu=0.3$  (Moeendarbary et al., 2013; Charras et al., 2001) was used for elasticity measurements.

### 2.6. Cellular poroelasticity measurement

As the cell size (> 30  $\mu$ m) was more than three orders of magnitude larger than the AFM tip radius (25 nm), the probe-cell interaction could

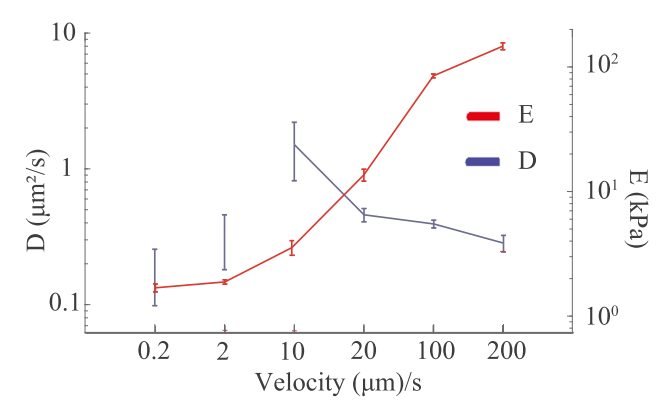


Fig. 5. Changes of cell poroelasticity and elasticity in response to change in indenting velocity.

be approximated as a poroelastic half-space indented by a conical indenter, and the following empirical poroelastic model obtained by finite-element-analysis was used for analyzing the cell poroelasticity (Hu et al., 2010):

$$\frac{F(t) - F_f}{F_i - F_f} = 0.493e^{-0.822}\sqrt{\frac{Dt}{a^2}} + 0.507e^{-1.348\frac{Dt}{a^2}}.$$
(3)

where  $F_i$  and  $F_j$  are the initial and final forces in the relaxation portion of the force-time curve, respectively. D is the diffusion coefficient. The probe-cell contact size, a, can be quantified using the indentation depth as:

$$a = \frac{2}{\pi} \overline{\delta} \tan(\alpha). \tag{4}$$

where  $\bar{\delta}$  is the indentation depth at the beginning of the force-relaxation process (i.e., the indentation caused by the displacement of the AFM piezo), and  $\alpha$  is the half opening angle of the conical shaped AFM probe.

# 2.7. Curve fitting and statistical analysis

Relaxation portions of collected force-time curves from AFM were fitted by the poroelastic model (Eq. (3)) using Matlab. Each force-re-laxation curve was fitted and the RMS fitting error was included in the results to demonstrate the measurement consistency.

#### 3. Results and discussion

#### 3.1. Poroelastic behavior of living cells

First, the experiment results validated the chosen empirical poroelasticity model and demonstrated that living cells exhibited poroelastic behavior. As shown in Fig. 4, the probe-cell interaction force started to decrease once the probe was rested on the cell surface following the indenting process, and went through a rapid exponential decay during the 1 s relaxation measurement. This observation is consistent with the previous studies on other cell types (Moeendarbary et al., 2013; Wu et al., 1998). Indeed, the poroelasticity model (Eq. (3)) fitted the force-relaxation curve well with the relative RMS fitting error ranging between 2.5-14%. These indicate that the force decrease during the relaxation corresponds to cellular poroelastic behavior. As can be seen in Figs. 4 (C) and (F), the force reduced by at least 50% on average for all of the measurements but the indentation increase was less than 6%, indicating that the force-relaxation data were collected under approximately constant applied intracellular strain. Therefore, the force relaxation (i.e., the force decrease) was primarily caused by intracellular fluid (e.g., cytosol) redistribution within the cytoplasm. Although the probe was rested in the cell following the indenting process, the applied compression on the cell caused the intracellular

liquid to move out of the probe-cell contact region through the porous structured cytoskeleton to equilibrate, and consequently, a reduction of the probe-cell interaction force.

To further study how the measurement conditions affect cell poroelasticity, we measured the force–relaxation curve under different indenting velocities and indentation depths.

#### 3.2. Effect of indenting velocity on poroelasticity of the cell

Six different indenting velocities (0.2, 2.0, 10.0, 20.0, 100.0, and 200.0 µm/s) were tested with the same targeted AFM indentation depth of 960 nm, and the force relaxation measurement was performed on at least six different cells for each velocity, respectively. The measured force relaxation curves were then fitted using Eq. (3), yielded a relative RMS fitting error in the range of 2.5-14% for all of the measurements. The results indicated that the cell poroelastic relaxation was more significant at higher indenting velocities. Specifically, as shown in Figs. 4 (C) and (F), the indentation increase and the force reduction were over 4% and 40%, with respect to their initial values (i.e., the indentation and force at the beginning of the relaxation), respectively, when the indenting velocity was higher than 10 µm/s. However, the indentation remained almost unchanged (with about 1% increase), and the force only decreased at most 23% for indenting velocities at 0.2 and  $2\,$   $\mu\text{m/s},$  indicating the probe-cell interaction was closer to equilibrium at the beginning of the one sec relaxation process-the end of the indenting process. In another word, the poroelastic relaxation phenomenon was more pronounced when the indenting velocity was higher than 10 µm/s. This is also confirmed by the normalized force-relaxation curve. The fitted force relaxation curves for different indenting velocities were normalized as  $(F(t) - F_f)/(F_i - F_f)$  as shown in Fig. 4 (D). The normalized force relaxation curves for the indenting velocities of 0.2 and 2 µm/s are above those for the higher velocities, especially after 0.2 s. Since higher normalized force values indicate less active intracellular fluid redistribution, the intracellular pressure was closer to equilibrium at the beginning of the relaxation process (i.e., at the end of the indenting process) when the cells were indented at 0.2 and 2  $\mu m/$ 

This observation can be explained using the empirical poroelastic model (Eq. (3)). According to Eq. (3), the poroelastic relaxation becomes more significant if the indenting velocity  $\nu$  is faster than the fluid efflux (Moeendarbary et al., 2013; Ibata et al., 2011), i.e.,  $v > \overline{\delta}/t_n$ where  $t_p$  is the timescale of the intracellular fluid movement and  $t_p \sim a^2/D$ . As the quantified diffusion coefficient (by fitting the forcerelaxation curve using Eq. (3)) for the targeted indentation  $\overline{\delta} \sim 960 \text{ nm}$ is in the range of 0.2–1.5  $\mu m^2/s$  (see Fig. 5), the indenting velocity for poroelastic relaxation measurement needs to satisfy v > 7 µm/s. This condition indicates that the intracellular fluid efflux can be negligible for all v> 7 µm/s velocities during the indenting process and contributes to the force reduction observed during the force relaxation process. Otherwise, significant intracellular fluid efflux can occur to equilibrate the inner pressure of the cell during the indenting process when  $v < 7 \mu m/s$ , and no much force reduction will be observed during the relaxation process. Therefore, the force relaxation immediately following rapid AFM indentation observed in this study was indeed caused by intracellular fluid efflux, and became more significant once the indenting velocity is faster than the fluid efflux rate. In particular, for the indenting velocities lower than 7 µm/s, the intracellular fluid flew out of the probe-cell contact region to equilibrate the pore pressure during the approaching process and soon reached equilibrium (steadystate), which resulted in barely changed force and indentation, i.e., the cell behavior was more elastic other than poroelastic, during the relaxation measurement. On the contrary, the intracellular fluid was not able to respond fast enough during rapid indentation ( $v > 7 \mu m/s$ ), and then the efflux started to occur once the probe was rested on the cell to equilibrate the intracellular pressure, causing a significant reduction of

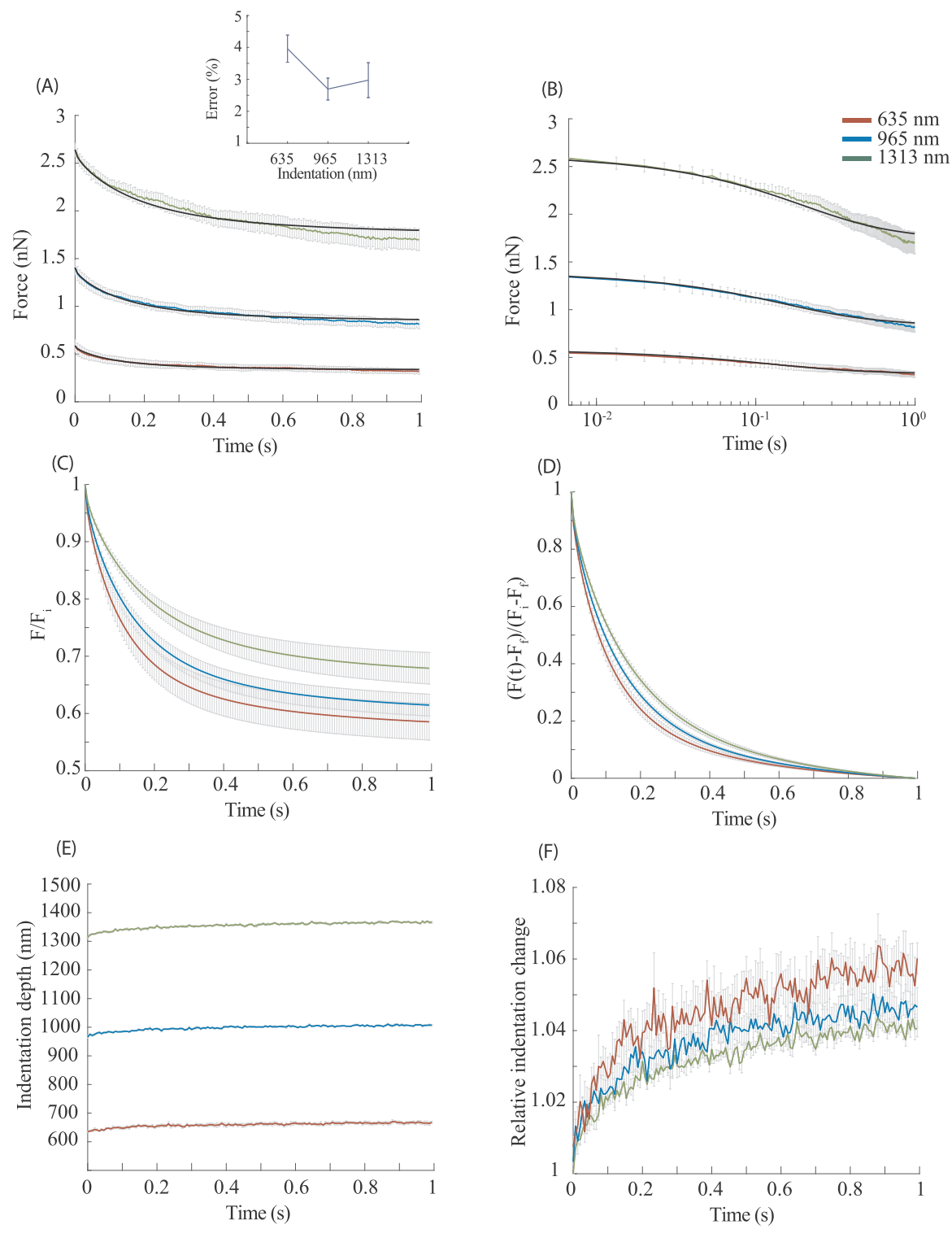


Fig. 6. (A) Force-relaxation curve for different indentation depths (635, 965, and 1313 nm) when the indenting velocity was 10  $\mu$ m/s. The mean value of the fitted curves for each velocity was shown as solid thick lines. The error bars denote the raw force data for each indenting velocity. (B) Log-Log plot of (A). (C) Relative force reduction during the relaxation process of the poroelastic fitted results in (A). (D) Normalized force reduction curve for different indentation depths when the indenting velocity was 10  $\mu$ m/s. At the same time instant, higher normalized value denotes slower intracellular fluid efflux. (E) Indentation change during the relaxation process: the indentation depth gradually increased when the probe was resting on the cell following the rapid indenting process. (F) Relative indentation change  $\delta/\bar{\delta}$  during the relaxation process.

the probe-cell interaction force. It is worth to note that by using nanometer-sized AFM probes the quantified diffusion coefficient in this study was smaller than those reported (in the range of 1–100  $\,\mu m^2/s)$  by using micro-beads on AFM (Moeendarbary et al., 2013).

To further study the relation between the cytoskeleton elasticity (i.e., Young's modulus) and cell poroelasticity, we fitted the force-

indentation curve with the Sneddon contact model (Eq. (2)) to quantify the Young's modulus, E, under different indenting velocities. The fitting results yielded E increasing from 1.5 kPa to 147 kPa monotonically with the indenting velocity increase as shown in Fig. 5. This monotonic E vs.  $\nu$  trend is consistent with previous results (Cheng) that as the cytoskeleton is highly viscoelastic and faster indenting velocities can increase

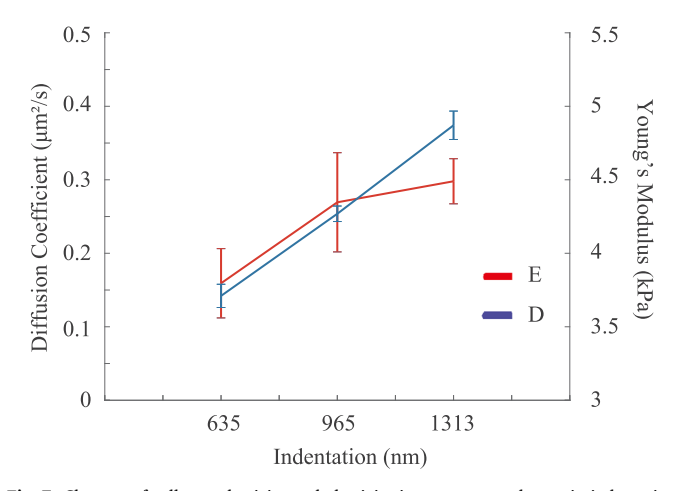
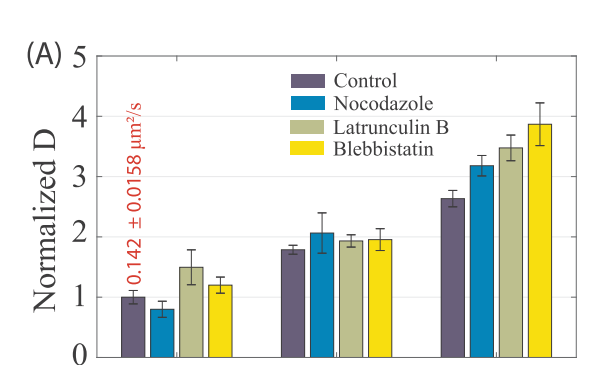


Fig. 7. Changes of cell poroelasticity and elasticity in response to change in indentation depth at the indenting velocity of 10  $\,\mu m/s$ .

the polymerization degree of the local actin, which further leads to local stiffening of the cytoskeleton (Rotsch and Radmacher, 2000; Moeendarbary et al., 2013). As a result, the increased actin polymerization and cytoskeleton stiffening may decrease the cytoskeleton pore size significantly, and further slows down the intracellular fluid efflux during the force relaxation process. This analysis can be confirmed by Fig. 4 (C), where the force reduction is smaller for higher indenting velocities during poroelastic relaxation for all v > 7 µm/s (note that the cases for v< 7 µm/s are excluded since fluid efflux happened even before the relaxation process started as discussed earlier). The trend of the quantified diffusion coefficient D (see Figs. 5) is also consistent with the above discussion, where D has an inverse relation with E for all  $v > 7 \mu m/s$ , as a higher value of D corresponds to more rapid fluid efflux. Note that this inverse relation between D and E doesn't conflict with the general recognized scaling law of diffusion coefficient:  $D \sim E\eta^2/\mu$ , where  $\eta$  is the pore radius of the cytoskeleton mesh work, and  $\mu$  is the viscosity of the intracellular fluid (i.e., cytosol). Although a higher approach velocity resulted in an increase of E, but the local cytoskeleton stiffening and actin polymerization caused the pore size  $\eta$  to decrease, and led to an overall smaller D. This indicates that change in  $\eta$  were more dominant than that of E in affecting the cytoplasm poroelasticity, and thereby, the cell rheology. As it is known that living cells are highly heterogeneous, and the cell shows high nonlinearity in terms of mechanical responses to external force excitation (Schillers et al., 2010; Fernández et al., 2006), next we investigated the nonlinearity of cell poroelasticity.



965

Indentation (nm)

635

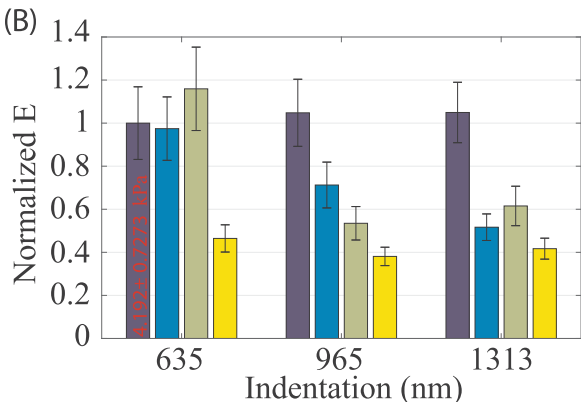


Fig. 8. Effect of microtubules depolymerization, F-actin depolymerization, and myosin inhibition on A) the diffusion coefficient and B) the Young's modulus under different indentation depth at the indenting velocity of  $10~\mu m/s$ .

1313

#### 3.3. Effect of indentation depth on poroelasticity of the cell

It has been studied that the structure heterogeneity may affect the mechanical behavior of living cells, e.g., stiffness and viscoelasticity (Kasas et al., 2005; Fuhrmann et al., 2011). Thus, we investigated the cell poroelasticity measured under three different indentation depths (635, 965, and 1313 nm) at the indenting velocity of  $10 \, \mu m/s$ .

As can be seen in Fig. 6, the cells showed poroelastic behavior at all indentation depths measured when the indenting velocity was 10 µm/ s. The poroelastic model fitted the force-relaxation curve well with a RMS fitting error less that 5% (Fig. 6 (A)), and the force reduction was more that 30% during the one sec relaxation process for all three indentation depths (Fig. 6 (B)) while the indentation remained nearly unchanged (Fig. 6 (E) and (F)). Moreover, the cell poroelasticity was indentation depth-dependent. The normalized  $((F(t) - F_f)/(F_i - F_f))$  curves collapse onto one master curve for all three indentation depth at time > 0.6 s (see Fig. 6 (D)); however, they are completely different for t< 0.6 s showing that the indentation depth affected the cell poroelastic relaxation during short time scale. This indicates that although the indenting velocity was kept the same, the change of indentation depth altered the cell's initial response of the relaxation process. Due to the multilayered structure of the cytoplasm, as the indentation depth increases, more layers of the cytoplasm (especially the cytoskeleton) could be excited and deformed during the indentation, and the measured cell mechanical response (poroelasticity and elasticity) changed accordingly. In particular, mainly the superficial layer of the cell (e.g., actin filament and cortical myosin II) deformed when the indentation depth was small (Schillers et al., 2010). At deeper indentations, more layers of the cytoplasm (e.g., bulky cytosol) may also be deformed along with the superficial layer. Therefore, distinct force-relaxation curves were observed at the beginning of the relaxation process, and then the force-relaxation curves collapsed together towards the end of the relaxation process, denoting that the intracellular pressure was close to equilibrium due to fluid efflux.

Different diffusion coefficient *D* and different Young's modulus *E* were obtained for the three measured indentation depths, respectively. A monotonic relation was observed between *E* and the indentation depth, and *E* increased by 30%, (see Fig. 7). This monotonic relation is consistent with previous findings that mammalian cells are not homogeneous in terms of elasticity (Schillers et al., 2010; Fernández et al., 2006). Particularly, the measured Young's modulus was determined by the elastic properties of both the superficial layer and the underneath second layer for deep indentation, and the latter had higher stiffness than the former (Schillers et al., 2010). In addition, stress stiffening of the cytoskeleton could also contribute to the Young's modulus increase for much deeper indentation. The elevated *E* for larger indentation depths indicated significant changes of the cytoskeleton structure, such as filament entanglement reinforcement (Moeendarbary et al., 2013;

Schillers et al., 2010). These structural changes together with the local cytoskeleton network stretching by deeper indentations could lead to significant increase of the cytoplasmic pore size  $\eta$ , which directly resulted in an increase of the diffusion coefficient. As confirmed by the results shown in Fig. 7, the diffusion coefficient D increased by 164% when the indentation depth increased from 635 to 1313 nm. This finding together with the aforementioned diffusion coefficient scaling law suggests that  $\eta$  was more dominant than E in affecting the cytoplasm poroelasticity.

# 3.4. Effect of cell cytoskeleton on cell poroelasticity

It has been reported that the components of cell cytoskeleton (e.g., actin filaments, microtubules, and myosin) affect the biomechanical behavior of the living cell (Rotsch and Radmacher, 2000; Schillers et al., 2010). Therefore, to understand the contribution of cytoskeleton on cell poroelasticity, the effects of actin filaments, microtubules, and myosin II on cell poroelasticity under different indentation depths (635, 965, and 1313 nm) at the indenting velocity of 10  $\mu\text{m/s}$  were investigated. The cells were treated with nocodazole (to depolymerize microtubules), latrunculin B (to depolymerize F-actin), and blebbistatin (to inhibit myosin II).

As can be seen in Fig. 8, nonlinearity of cell poroelasticity was more pronounced on the cells treated by the three drugs. Specifically, the diffusion coefficient of the cells treated with 5  $\mu$  M nocodazole increased from 0.11 to 0.45  $\,\mu m^2/s$  (increased by 309%) when the indentation was increased from 635 to 1313 nm, comparing with the control 0.14-0.37 µm<sup>2</sup>/s, a 164% increase). Depolymerization of the microtubules did not affect the measured D and E significantly when the indentation was relatively small (635 nm). This result agrees with the previous finding that microtubules had no significant effect on cell poroelasticity when the indentation was small (less than 800 nm) (Moeendarbary et al., 2013). However, the effect of microtubule depolymerization became more and more significant as the indentation depth increased-resulted in a 22% increase in the diffusion coefficient and a 51% decrease in the Young's modulus compared with the control at the indentation of 1313 nm. This observation revealed that microtubulues are more concentrated at deeper layers of the cytoskeleton (i.e., underneath the superficial layer), and thus its effect on cell mechanics can only be observed when the indentation depth is deep enough. Since depolymerization of the microtubules directly weakens the strength (i.e., stiffness) of the cytoskeleton, and results in an increase of the pore size, therefore, the diffusion coefficient was increased at all measured indentation depths compared with the control, and the opposite trend was observed for the Young's modulus. Furthermore, the deeper the indentation was, the more significant the microtubules effect was, thus, the changes of the diffusion coefficient and the Young's modulus were more significant. Note that due to the limited indentation depths used in previous studies, the effect of microtobulues on cell poroelasticity has never been reported before. Depolymerization of Factin resulted in an overall increased diffusion coefficient and significantly decreased Young's modulus for all indentation depths measured (with respect to the control at each indentation) and treatment of cells with blebbistatin resulted in more significant increases in both the diffusion coefficient and the Young's modulus. These changes of the Young's modulus and the diffusion coefficient of the perturbed cells are consistent with previous studies (Moeendarbary et al., 2013; Rotsch and Radmacher, 2000; Schillers et al., 2010) as depolymerization of F-actin and inhibition of myosin II activity contribute to reduction of cytoskeleton stiffness and increase of the cytoplasmic pore size. The change of the diffusion coefficient under these two treatments was quite notable at the indentation of 635 nm (50% for latrunculin B and 20% for blebbistatin) and became more significant as the indentation increased (at least 248% for both drugs at 1313 nm indentation). This indicates that depolymerization of F-actin and inhibition of myosin II can cause structural changes at both the superficial and the deeper layers of the cell cytoskeleton, and these structural changes are more significant as the indentation depth increases.

Beside the drug treatment effects, nonlinearity of the diffusion coefficient (i.e., the indentation depth-dependence) of the treated cells was also resulted from the stretching of the cytoskeleton network as discussed earlier. It is worth to note that the diffusion coefficient and the Young's modulus of the control are close to those of the cells measured in the L-15 medium without DMSO at the same velocity and the indentations (see Fig. 7), therefore, the change of cell poroelasticity of the treated cells was indeed caused by the cytoskeleton treatments other than DMSO. Taken together, these results revealed that F-actin and myosin II plays a fundamental role in modulating cellular rheology, and myosin II plays a more dominant role in affecting the cytoplasm elasticity (i.e., Young's modulus). Moreover, the opposite trends of the diffusion coefficient and the Young's modulus changes confirmed that the cytoplasmic pore size dominates over elasticity in determining cell rheology.

#### 4. Conclusion

In this study, the nanoscale cell poroelasticity was investigated using AFM indentation approach. Velocity-dependence and the nonlinearity of MDA-MB-231 cell poroelastic behavior was quantified by quantifying the diffusion coefficient through fitting the force-relaxation curves with the poroelastic model. Moreover, the effects of actin filaments, microtubules, and myosin II on the cell elastic and poroelastic behavior was studied. It was found that the cell had poor poroelastic behavior when the indenting velocity was lower than 10 µm/s due to intracellular fluid redistribution within the cell during indentation. Lower diffusion coefficient for faster indenting velocities confirmed poor poroelastic behavior of the cell due to local stiffening of the cell at faster velocity. Deeper indentation led to higher diffusion coefficient and more efficient poroelastic relaxation of the cell due to the increases of the cytoplasmic pore size and cell stiffness. Inhibition of the aforementioned cytoskeletal components resulted in significant increase of the diffusion coefficient and dramatic decrease of the Young's modulus compared with the control. Differences of the three cytoskeleton inhibition treatments in affecting the nonlinearity of cell poroelasticity revealed that F-actin and myosin II affects cytoskeleton structure at both the superficial and the deeper layers, while microtubule is mainly affects the cell mechanical behavior at the deeper layers of the cytoskeleton.

#### Acknowledgements

This work was supported by the National Science Foundation (NSF) [CMMI-1634592], and Iowa State University. The authors also thank Dr. Ian Schneider for providing MDA-MB-231 cells.

#### References

Bachrach, N.M., Valhmu, W.B., Stazzone, E., Ratcliffe, A., Lai, W.M., Mow, V.C., 1995. Changes in proteoglycan synthesis of chondrocytes in articular cartilage are associated with the time-dependent changes in their mechanical environment. J. Biomech. 28 (12), 1561–1569.

Balaban, N.Q., Schwarz, U.S., Riveline, D., Goichberg, P., Tzur, G., Sabanay, I., Mahalu, D., Safran, S., Bershadsky, A., Addadi, L., et al., 2001. Force and focal adhesion assembly: a close relationship studied using elastic micropatterned substrates. Nat. Cell Biol. 3 (5), 466–472.

Brandao, M., Fontes, A., Barjas-Castro, M., Barbosa, L., Costa, F., Cesar, C., Saad, S., 2003. Optical tweezers for measuring red blood cell elasticity: application to the study of drug response in sickle cell disease. Eur. J. Haematol. 70 (4), 207–211.

Butt, H.-J., Cappella, B., Kappl, M., 2005. Force measurements with the atomic force microscope: technique, interpretation and applications. Surf. Sci. Rep. 59 (1), 1–152. Charras, G., Lehenkari, P.P., Horton, M., 2001. Atomic force microscopy can be used to

narras, G., Lenenkari, P.P., Horton, M., 2001. Atomic force microscopy can be use mechanically stimulate osteoblasts and evaluate cellular strain distributions. Ultramicroscopy 86 (1), 85–95.

Charras, G.T., Yarrow, J.C., Horton, M.A., Mahadevan, L., Mitchison, T., 2005. Non-equilibration of hydrostatic pressure in blebbing cells. Nature 435 (7040), 365–369. Charras, G.T., Coughlin, M., Mitchison, T.J., Mahadevan, L., 2008. Life and times of a

- cellular bleb. Biophys. J. 94 (5), 1836-1853.
- Charras, G.T., Mitchison, T.J., Mahadevan, L., 2009. Animal cell hydraulics. J. Cell Sci. 122 (18), 3233–3241.
- Cheng, A.H.-D., Fundamentals of poroelasticity, Analysis and Design Methods: Comprehensive Rock Engineering: Principles, Practice and Projects 113.
- Chu, Y.-S., Dufour, S., Thiery, J.P., Perez, E., Pincet, F., 2005. Johnson-kendall-roberts theory applied to living cells. Phys. Rev. Lett. 94 (2), 028102.
- Coller, H.A., Grandori, C., Tamayo, P., Colbert, T., Lander, E.S., Eisenman, R.N., Golub, T.R., 2000. Expression analysis with oligonucleotide microarrays reveals that myc regulates genes involved in growth, cell cycle, signaling, and adhesion. Proc. Natl. Acad. Sci. USA 97 (7), 3260–3265.
- Colombelli, J., Besser, A., Kress, H., Reynaud, E.G., Girard, P., Caussinus, E., Haselmann, U., Small, J.V., Schwarz, U.S., Stelzer, E.H., 2009. Mechanosensing in actin stress fibers revealed by a close correlation between force and protein localization. J. Cell Sci. 122 (10), 1665–1679.
- Derjaguin, B.V., Muller, V.M., Toporov, Y.P., 1975. Effect of contact deformations on the adhesion of particles. J. Colloid Interface Sci. 53 (2), 314–326.
- Dong, C., Skalak, R., Sung, K., 1990. Cytoplasmic rheology of passive neutrophils. Biorheology 28 (6), 557–567.
- Drury, J.L., Dembo, M., 1999. Hydrodynamics of micropipette aspiration. Biophys. J. 76 (1), 110–128.
- Drury, J.L., Dembo, M., 2001. Aspiration of human neutrophils: effects of shear thinning and cortical dissipation. Biophys. J. 81 (6), 3166–3177.
- Efremov, Y.M., Wang, W.-H., Hardy, S.D., Geahlen, R.L., Raman, A., 2017. Measuring nanoscale viscoelastic parameters of cells directly from afm force-displacement curves. Sci. Rep. 7 (1), 1541.
- Evans, E., Kukan, B., 1984. Passive material behavior of granulocytes based on large deformation and recovery after deformation tests. Blood 64 (5), 1028–1035.
- Fabry, B., Maksym, G.N., Butler, J.P., Glogauer, M., Navajas, D., Fredberg, J.J., 2001. Scaling the microrheology of living cells. Phys. Rev. Lett. 87 (14), 148102.
- Fernández, P., Pullarkat, P.A., Ott, A., 2006. A master relation defines the nonlinear viscoelasticity of single fibroblasts. Biophys. J. 90 (10), 3796–3805.
- Fredberg, J.J., Stamenovic, D., 1989. On the imperfect elasticity of lung tissue. J. Appl. Physiol. 67 (6), 2408–2419.
- Fuhrmann, A., Staunton, J., Nandakumar, V., Banyai, N., Davies, P., Ros, R., 2011. Afm stiffness nanotomography of normal, metaplastic and dysplastic human esophageal cells. Phys. Biol. 8 (1), 015007.
- Gao, H., Yao, H., 2004. Shape insensitive optimal adhesion of nanoscale fibrillar structures. Proc. Natl. Acad. Sci. USA 101 (21), 7851–7856.
- Ghaednia, H., Marghitu, D.B., Jackson, R.L., 2015a. Predicting the permanent deformation after the impact of a rod with a flat surface. J. Tribology 137 (1), 011403.
- Ghaednia, H., Cermik, O., Marghitu, D.B., 2015b. Experimental and theoretical study of the oblique impact of a tennis ball with a racket. Proc. Inst. Mech. Eng., Part P. J. Sports Eng. Technol. 229 (3), 149–158.
- Ghaednia, H., Pope, S.A., Jackson, R.L., Marghitu, D.B., 2016. A comprehensive study of the elasto-plastic contact of a sphere and a flat. Tribology Int. 93, 78–90.
- Giridharagopal, R., Rayermann, G.E., Shao, G., Moore, D.T., Reid, O.G., Tillack, A.F., Masiello, D.J., Ginger, D.S., 2012. Submicrosecond time resolution atomic force microscopy for probing nanoscale dynamics. Nano Lett. 12 (2), 893–898.
- Gu W., Lai W., Hung C., Liu Z., Mow V., 1997. Analysis of transient swelling and electrical responses of an isolated cell to sudden osmotic loading, In: American Society of Mechanical Engineers, Bioengineering Division (Publication) BED.
- Guilak, F., Mow, V.C., 2000. The mechanical environment of the chondrocyte: a biphasic finite element model of cell-matrix interactions in articular cartilage. J. Biomech. 33 (12), 1663–1673.
- Hayakawa, K., Tatsumi, H., Sokabe, M., 2008. Actin stress fibers transmit and focus force to activate mechanosensitive channels. J. Cell Sci. 121 (4), 496–503.
- Hayakawa, K., Tatsumi, H., Sokabe, M., 2011. Actin filaments function as a tension sensor by tension-dependent binding of cofilin to the filament. J. Cell Biol. 195 (5), 721–727
- Hildebrandt, J., 1969. Comparison of mathematical models for cat lung and viscoelastic balloon derived by laplace transform methods from pressurevolume data. Bull. Math. Biol. 31 (4), 651–667.
- Hochmuth, R., Ting-Beall, H., Beaty, B., Needham, D., Tran-Son-Tay, R., 1993. Viscosity of passive human neutrophils undergoing small deformations. Biophys. J. 64 (5), 1596–1601.
- Hu, Y., Zhao, X., Vlassak, J.J., Suo, Z., 2010. Using indentation to characterize the poroelasticity of gels. Appl. Phys. Lett. 96 (12), 121904.
- Hutter, J.L., Bechhoefer, J., 1993. Calibration of atomic-force microscope tips. Rev. Sci. Instrum. 64 (7), 1868–1873.
- Ibata, K., Takimoto, S., Morisaku, T., Miyawaki, A., Yasui, M., 2011. Analysis of aquaporin-mediated diffusional water permeability by coherent anti-stokes raman scattering microscopy. Biophys. J. 101 (9), 2277–2283.
- Jackson, R.L., Ghaednia, H., Pope, S., 2015. A solution of rigid-perfectly plastic deep spherical indentation based on slip-line theory. Tribology Lett. 58 (3), 47.
- Johnson K., Kendall K., A. Roberts, Surface energy and the contact of elastic solids, In: Proceedings of the Royal Society of London A: Mathematical, Physical and Engineering Sciences, vol. 324, The Royal Society, 1971, pp. 301–313.
- Kalcioglu, Z.I., Mahmoodian, R., Hu, Y., Suo, Z., Vliet, K.J.Van, 2012. From macro-to microscale poroelastic characterization of polymeric hydrogels via indentation. Soft

- Matter 8 (12) 3393-3398
- Kardel, K., Ghaednia, H., Carrano, A.L., Marghitu, D.B., 2017. Experimental and theoretical modeling of behavior of 3d-printed polymers under collision with a rigid rod. Addit. Manuf. 14, 87–94.
- Kasas, S., Wang, X., Hirling, H., Marsault, R., Huni, B., Yersin, A., Regazzi, R., Grenningloh, G., Riederer, B., Forro, L., et al., 2005. Superficial and deep changes of cellular mechanical properties following cytoskeleton disassembly. Cytoskeleton 62 (2) 124–132
- Keren, K., Yam, P.T., Kinkhabwala, A., Mogilner, A., Theriot, J.A., 2009. Intracellular fluid flow in rapidly moving cells. Nat. Cell Biol. 11 (10), 1219–1224.
- Lim, C., Zhou, E., Quek, S., 2006. Mechanical models for living cells-a review. J. Biomech. 39 (2), 195–216.
- Liu, K.-K., 2006. Deformation behaviour of soft particles: a review. J. Phys. D: Appl. Phys. 39 (11). R189.
- Maksym, G.N., Fabry, B., Butler, J.P., Navajas, D., Tschumperlin, D.J., Laporte, J.D., Fredberg, J.J., 2000. Mechanical properties of cultured human airway smooth muscle cells from 0.05 to 0.4 hz. J. Appl. Physiol. 89 (4), 1619–1632.
- Maloney, J.M., Nikova, D., Lautenschläger, F., Clarke, E., Langer, R., Guck, J., Van Vliet, K.J., 2010. Mesenchymal stem cell mechanics from the attached to the suspended state. Biophys. J. 99 (8), 2479–2487.
- Mikulich A., Kavaliauskiene S., Juzenas P. 2012. Blebbistatin, a myosin inhibitor, is phototoxic to human cancer cells under exposure to blue light, Biochimica et Biophysica Acta (BBA)-General Subjects 1820 (7) 870-877.
- Mitrossilis, D., Fouchard, J., Guiroy, A., Desprat, N., Rodriguez, N., Fabry, B., Asnacios, A. 2009. Single-cell response to stiffness exhibits muscle-like behavior, Proceedings of the National Academy of Sciences 106 (43) 18243-18248.
- Moeendarbary, E., Harris, A.R., 2014. Cell mechanics: principles, practices, and prospects. Wiley Interdiscip. Rev.: Syst. Biol. Med. 6 (5), 371–388.
- Moeendarbary, E., Valon, L., Fritzsche, M., Harris, A.R., Moulding, D.A., Thrasher, A.J., Stride, E., Mahadevan, L., Charras, G.T., 2013. The cytoplasm of living cells behaves as a poroelastic material. Nat. Mater. 12 (3), 253–261.
- Nia, H.T., Han, L., Li, Y., Ortiz, C., Grodzinsky, A., 2011. Poroelasticity of cartilage at the nanoscale. Biophys. J. 101 (9), 2304–2313.
- Niclas, J., Allan, V.J., Vale, R.D., 1996. Cell cycle regulation of dynein association with membranes modulates microtubule-based organelle transport. J. Cell Biol. 133 (3), 585–594.
- Oster, G., 1989. Cell Motility and Tissue Morphogenesis. Academic Press, New York. Plotnikov, S.V., Pasapera, A.M., Sabass, B., Waterman, C.M., 2012. Force fluctuations within focal adhesions mediate ecm-rigidity sensing to guide directed cell migration. Cell 151 (7). 1513–1527.
- Ren, J., Yu, S., Gao, N., Zou, Q., 2013. Indentation quantification for in-liquid nanomechanical measurement of soft material using an atomic force microscope: ratedependent elastic modulus of live cells. Phys. Rev. E 88 (5), 052711.
- Ren, J., Huang, H., Liu, Y., Zheng, X., Zou, Q., 2015. An atomic force microscope study revealed two mechanisms in the effect of anticancer drugs on rate-dependent young's modulus of human prostate cancer cells. PloS One 10 (5), e0126107.
- Rosenbluth, M.J., Crow, A., Shaevitz, J.W., Fletcher, D.A., 2008. Slow stress propagation in adherent cells. Biophys. J. 95 (12), 6052–6059.
- Rotsch, C., Radmacher, M., 2000. Drug-induced changes of cytoskeletal structure and mechanics in fibroblasts: an atomic force microscopy study. Biophys. J. 78 (1), 520–535
- S. J. Elledge, Cell cycle checkpoints: preventing an identity crisis, Science 274 (5293) (1996) 1664.
- Schillers, H., Wälte, M., Urbanova, K., Oberleithner, H., 2010. Real-time monitoring of cell elasticity reveals oscillating myosin activity. Biophys. J. 99 (11), 3639–3646.
- Sneddon, I.N., 1965. The relation between load and penetration in the axisymmetric boussinesq problem for a punch of arbitrary profile. Int. J. Eng. Sci. 3 (1), 47–57.
- Sun, Y., Villa-Diaz, L.G., Lam, R.H., Chen, W., Krebsbach, P.H., Fu, J., 2012. Mechanics regulates fate decisions of human embryonic stem cells. PLoS One 7 (5), e37178.
- Sung, K.-L.P., Schmid-Schb'nbein, G., Chien, S., 1988. Passive deformation analysis of human leukocytes. J. Biomech. Eng. 110, 27.
- Tran-Son-Tay, R., Needham, D., Yeung, A., Hochmuth, R., 1991. Time-dependent recovery of passive neutrophils after large deformation. Biophys. J. 60 (4), 856–866.
- Weafer, P., Reynolds, N., Jarvis, S., McGarry, J., 2015. Single cell active force generation under dynamic loading-part i: afm experiments. Acta Biomater. 27, 236–250.
- Wu, H., Kuhn, T., Moy, V., 1998. Mechanical properties of 1929 cells measured by atomic force microscopy: effects of anticytoskeletal drugs and membrane crosslinking. Scanning 20 (5), 389–397.
- Wu S., Polymer interface and adhesion, M. Dekker, 1982.
- Yan, B., Ren, J., Zheng, X., Liu, Y., Zou, Q., 2017. High-speed broadband monitoring of cell viscoelasticity in real time shows myosin-dependent oscillations. Biomech. Model. Mechanobiol. 1–12.
- Yeung, A., Evans, E., 1989. Cortical shell-liquid core model for passive flow of liquid-like spherical cells into micropipets. Biophys. J. 56 (1), 139–149.
- Zhu, X., Siamantouras, E., Liu, K.-K., Liu, X., 2016. Determination of work of adhesion of biological cell under afm bead indentation. J. Mech. Behav. Biomed. Mater. 56, 77–86.
- Zicha, D., Dobbie, I.M., Holt, M.R., Monypenny, J., Soong, D.Y., Gray, C., Dunn, G.A., 2003. Rapid actin transport during cell protrusion. Science 300 (5616), 142–145.